TISSUE ENGINEERING: Part A
Volume 17, Numbers 11 and 12, 2011

DOI: 10.1089/ten.tea.2010.0573

Lamellar Spacing in Cuboid Hydroxyapatite Scaffolds Regulates Bone Formation by Human Bone Marrow Stromal Cells

Mahesh H. Mankani, M.D.,[1] Shahrzad Afghani, B.S.,[1] Jaime Franco, Ph.D.,[2] Max Launey, Ph.D.,[2] Sally Marshall, Ph.D.,[3] Grayson W. Marshall, D.D.S., M.P.H., Ph.D.,[3] Robert Nissenson, Ph.D.,[4] Janice Lee, D.D.S., M.D., M.S.,[5] Antoni P. Tomsia, Ph.D.,[2] and Eduardo Saiz, Ph.D.[2,6]

Background: A major goal in bone engineering is the creation of large volume constructs (scaffolds and stem cells) that bear load. The scaffolds must satisfy two competing requirements—they need be sufficiently porous to allow nutrient flow to maintain cell viability, yet sufficiently dense to bear load. We studied the effect of scaffold macroporosity on bone formation and scaffold strength, for bone formed by human bone marrow stromal cells.
Methods: Rigid cubical hydroxyapatite/tricalcium phosphate scaffolds were produced by robo-casting. The ceramic line thickness was held constant, but the distance between adjacent lines was either 50, 100, 200, 500, or 1000 μm. Cultured human bone marrow stromal cells were combined with the scaffolds *in vitro*; transplants were placed into the subcutis of immunodeficient mice. Transplants were harvested 9, 18, 23, 38, or 50 weeks later. Bone formation and scaffold strength were analyzed using histology and compression testing.
Results: Sixty transplants were evaluated. Cortical bone increased with transplant age, and was greatest among 500 μm transplants. In contrast, maximum transplant strength was greatest among 200 μm transplants.
Conclusions: Lamellar spacing within scaffolds regulates the extent of bone formation; 500 μm yields the most new bone, whereas 200 μm yields the strongest transplants.

Introduction

The ultimate goal in the engineering of new bone is the formation of large volume, weight-bearing constructs. Thus far, large volume transplants made with particulate scaffolds have successfully closed defects in large animal models.[1] The next threshold in this process is the creation of scaffolds that bear weight while simultaneously supporting transplanted skeletal stem cells. A major limitation to successful cell transplantation in this setting is the difficulty in providing nutritional support to the cells in the interior of the scaffold. These cells are typically supported by diffusion of nutrients from the periphery during the short term, and by vascularization over the long term. The scaffold must therefore satisfy two competing primary design requirements—it must be porous enough to allow nutrient flow to maintain cell viability, and yet it must be dense enough to bear loads. Additional but less critical design parameters include (1) the capability to undergo programmed resorption, and (2) the ability to bind and eventually release angiogenic growth factors.

Although these competing requirements are well recognized, a detailed examination of the effect of scaffold macroporosity has not been completed. For our purposes, porosity may be sub-divided according to its scale. Microporosity refers to pores on the micrometer and submicrometer scale, while macroporosity reflects pore sizes ranging from 20 μm to 1 mm. Microporosity, in association with surface roughness, influences osteoblast adhesion and differentiation. In contrast, macroporosity influences the density of adherent cells and the ability of capillaries and larger caliber vessels to grow into the scaffold.

The purpose of this study was to evaluate bone formation and scaffold strength as a function of macroporosity. Novel hydroxyapatite/tricalcium phosphate (HA/TCP) lattice-work

[1]Department of Surgery, University of California–San Francisco, San Francisco, California.
[2]Materials Sciences Division, Lawrence Berkeley National Laboratory, Berkeley, California.
[3]Preventive and Restorative Dental Sciences, University of California–San Francisco, San Francisco, California.
[4]Endocrine Unit, VA Medical Center (111N), Departments of Medicine and Physiology, University of California–San Francisco, San Francisco, California.
[5]Department of Oral and Maxillofacial Surgery, University of California–San Francisco, San Francisco, California.
[6]Department of Materials, Center for Advanced Structural Ceramics, UK Center for Structural Ceramics, Imperial College, Royal School of Mines, London, United Kingdom.

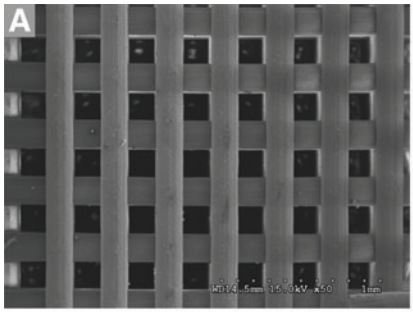
A

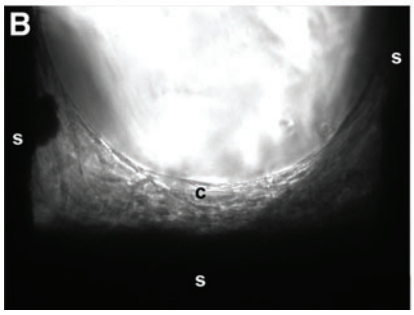
B
s
s
c
s

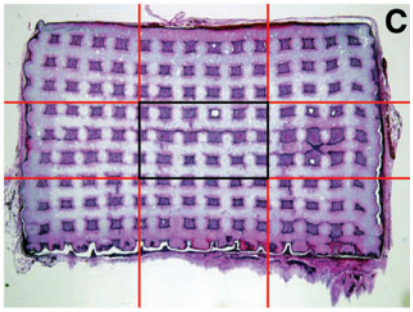
C

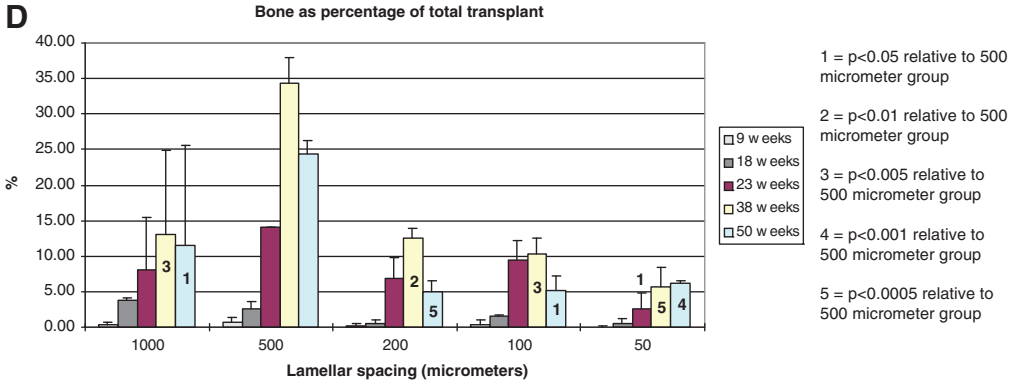
D
Bone as percentage of total transplant
%
40.00
35.00
30.00
25.00
20.00
15.00
10.00
5.00
0.00
1000
500
200
100
50
Lamellar spacing (micrometers)
9 w eeks
18 w eeks
23 w eeks
38 w eeks
50 w eeks
1 = p<0.05 relative to 500 micrometer group
2 = p<0.01 relative to 500 micrometer group
3 = p<0.005 relative to 500 micrometer group
4 = p<0.001 relative to 500 micrometer group
5 = p<0.0005 relative to 500 micrometer group

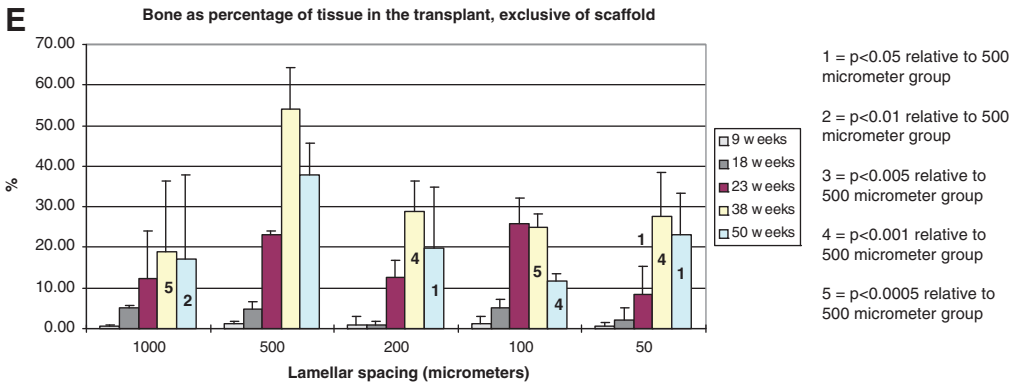
E
Bone as percentage of tissue in the transplant, exclusive of scaffold
%
70.00
60.00
50.00
40.00
30.00
20.00
10.00
0.00
1000
500
200
100
50
Lamellar spacing (micrometers)
9 w eeks
18 w eeks
23 w eeks
38 w eeks
50 w eeks
1 = p<0.05 relative to 500 micrometer group
2 = p<0.01 relative to 500 micrometer group
3 = p<0.005 relative to 500 micrometer group
4 = p<0.001 relative to 500 micrometer group
5 = p<0.0005 relative to 500 micrometer group

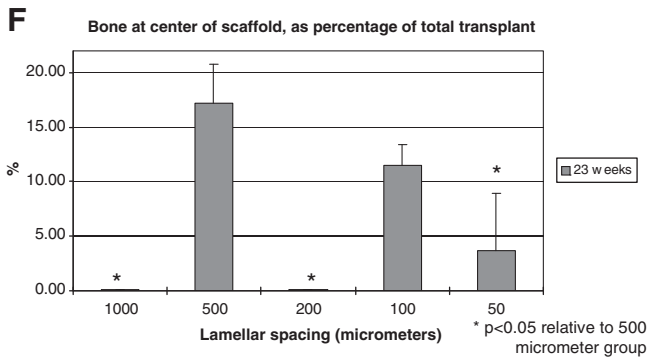
F
Bone at center of scaffold, as percentage of total transplant
%
20.00
15.00
10.00
5.00
0.00
1000
500
200
100
50
Lamellar spacing (micrometers)
23 w eeks
* p<0.05 relative to 500 micrometer group

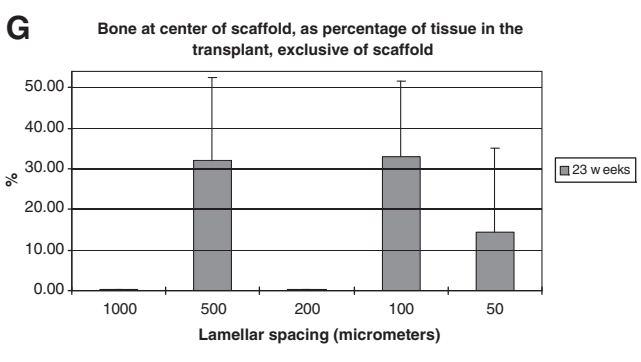
G
Bone at center of scaffold, as percentage of tissue in the transplant, exclusive of scaffold
%
50.00
40.00
30.00
20.00
10.00
0.00
1000
500
200
100
50
Lamellar spacing (micrometers)
23 w eeks

scaffolds were constructed using robocasting such that the macroporosity ranged from 50 to 1000 μm in a controlled fashion. Scaffolds were seeded with preset numbers of culture-expanded human bone marrow stromal cells (hBMSCs), placed into the subcutis of Bg-Nu-XID mice, harvested at time points ranging from 9 to 50 weeks, and analyzed via histomorphometry and strength testing.

Materials and Methods

Scaffold preparation

Ceramic-based inks for robocasting were prepared by dispersing mixtures of HA powder (Trans-Tech) and TCP powder (Keramat) (65/35 wt%) with an average particle size of 2.4 μm in Pluronic® F-127 water-based solutions with Pluronic contents ranging between 10 and 30 wt%. The dispersion of the ceramic powders was performed inside an ice/water bath to reverse the gellation process and reduce the viscosity.[2] Approximately 2.5 wt% of 1-Octanol (Sigma-Aldrich) in water was added to the mixture to minimize the presence of bubbles. The suspensions were homogenized using an 800W stirrer with variable speed (Dewalt DW236, 0–800 rpm). After dispersing the powders, 4 wt% of commercial corn syrup in water was added to the ink to enhance the adhesion between printed layers. The ink was mixed thoroughly for 10 min and sieved afterward through a 100 μm nylon mesh to achieve optimum homogenization and minimize the presence of particle aggregates. The inks were loaded into a 10 mL syringe (BD) that was gently tapped to eliminate air bubbles.

The inks were used to print standard ceramic grids with a robotic deposition device (Robocad 3.0, 3-D Inks). The diameter of the printing nozzle was 250 μm. (EFD-precision tips, RI). The grids were printed inside a reservoir of nonwetting oil (Lamplight®) on an aluminum oxide plate of 1 mm thickness. To avoid deformations due to uneven shrinkage during drying and sintering, a layer of permanent marker (Sharpie; Sandford) was applied on the surface of the alumina sheet followed by a second layer of commercial corn syrup deposited by spin coating (WS-400B-6NPP-LITE; Laurell Technologies Corporation). After printing, the plates were tilted ~45° to remove the excess oil and dried for 24 h at room temperature. The pieces were fired at 600°C (1°C.min^{-1}, heating rate) for 2 h to evaporate the organics, followed by sintering for 2 h at 1275°C with a heating and cooling rate of 5°C.min^{-1}. The composition and microstructure of the sintered grids were characterized by X-ray diffraction and scanning electron microscopy. After sintering, the grids consisted of printed lines of ~200 μm diameter with pore sizes varying systematically between 50 and 1000 μm. The printed lines had ~10 vol% of microporosity with micro-pore sizes in the micrometer range. Scaffold structures measuring 8×8×5 mm were produced using these techniques (Fig. 1A).

Transplant preparation, placement, and recovery

Surgical specimens were obtained containing fragments of normal unaffected bone with bone marrow from a patient undergoing reconstructive surgery. The male patient, aged 19 years, underwent iliac crest bone harvest for an orthopedic reconstructive procedure. Tissue procurement proceeded in accordance with NIH regulations governing the use of human subjects (Protocols 94-D-0188). Multi-colony-derived strains of BMSCs were derived from the bone marrow in a manner previously described.[3] Briefly, a single-cell suspension of bone marrow cells was cultured in growth medium consisting of αMEM, 2 mM L-glutamine, 100 U/mL penicillin, 100 μg/mL streptomycin sulfate (Invitrogen), 10^{-8} M dexamethasone (Sigma), 10^{-4} M L-ascorbic acid phosphate magnesium salt n-hydrate (Wako), and 20% fetal bovine serum of a preselected lot (Equitech-Bio, Inc.). In our hands, 20% fetal bovine serum promotes faster cell proliferation without inducing cellular senescence. After 24 h, nonadherent cells were removed by extensive washing. The cells were then incubated at 37°C in an atmosphere of 100% humidity and 5% CO_2. The medium was changed weekly following initial plating, when the cell density in the tissue culture flasks was of such low density that the media remained at a physiologic pH during the entire week. For subsequent passaging, when cell density was substantially higher in the flasks, cells underwent either passaging or media change approximately every 3 days. Cells at passage 3 were cryo-preserved in liquid nitrogen. For this set of studies, a single vial containing 2.0 million cells was thawed, plated, and further passaged until sufficient cells were available.

Upon approaching confluence at passage 5, BMSCs were trypsin-released and transferred to Falcon six-well plates, each well receiving 1 million BMSCs and a set of 5 scaffolds representing the different lamellar spacing. BMSCs were permitted to adhere and proliferate on the scaffolds. Cells were found to adhere and proliferate on the scaffolds within a day of plating, forming multilayer networks within 3 days (Fig. 1B). After 1 week, the scaffolds were recovered from the plates and transplanted.

Eight-month-old immunocompromised Bg-Nu/Nu-Xid female mice (Harlan-Sprague Dawley) served as transplant recipients. All animals were cared for according to the policies and principles established by the Animal Welfare Act and the NIH Guide for the Care and Use of Laboratory Animals. Operations were performed in accordance to specifications of an approved UCSF animal research protocol (AN077250). Mice were anesthetized with inhalational isoflurane and oxygen. Transplants were placed in the subcutaneous space along the back, with each mouse receiving all five types of scaffolds. Incisions were closed with suture. Twelve mice were given a total of 60 transplants. The mice were sacrificed at 9, 18, 23, 38, or 50 weeks postoperatively with inhaled CO_2 and their transplants harvested.

FIG. 1. **(A)** Scanning electron microscopic image of 200 μm scaffold before culture. **(B)** Transmission light microscopic image of a scaffold 3 days after seeding with human BMSCs. (s, scaffold; c, BMSCs). **(C)** Demonstration of center 1/9th of transplant, depicted by the area enclosed by the center black rectangle. **(D)** Percentage of bone within the entire transplant, including both transplant periphery and center. **(E)** Percentage of bone within the tissue (nonscaffold) portions of the transplant. Transplant periphery and center are both included. **(F)** Percentage of bone within the center of the transplant. **(G)** Percentage of bone within the tissue (nonscaffold) portions of the transplant, taken only from the transplant center. BMSC, bone marrow stromal cells. Color images available online at www.liebertonline.com/tea

Histomorphometry of bone sections

All of the transplants were fixed in 4% phosphate-buffered formalin freshly prepared from paraformaldehyde. Following an overnight fixation at 4°C, the transplants were suspended in phosphate-buffered saline. The transplants were demineralized in buffered 10% EDTA, dehydrated, embedded in paraffin, and sectioned. Sections were deparaffinized, hydrated, and stained with hematoxylin and eosin.

A single section from the interior of each transplant was obtained, stained with hematoxylin and eosin, and examined to quantify the areas that had either formed or not formed bone. Areas of bone formation (B) were easily distinguished from the scaffold (S), fibro-vascular tissue (FV), and hematopoietic tissue (H). B, S, FV, H, and the total transplant area (T) were then measured for each section. As expected, B + S + FV + H=T. All histologic images were magnified using a Zeiss Axioplan microscope (Zeiss), and they were captured using the microscope-imaging program Spot Advanced (Diagnostic Instruments, Inc.). Area measurements were obtained with ImageJ version 1.36 (National Institutes of Health). The B, S, FV, H, and T values of the sections for each transplant were averaged to compute an overall set of values for each transplant.

The transplants harvested at 23 weeks were further analyzed to quantify bone formation within the interior-most portion of the transplant. Each transplant was divided into nine equal portions using a 3×3 grid, and the center-most portion was assessed for the amount of bone formation (Fig. 1C).

Statistical comparisons of average outcome levels between groups characterized by scaffold size and sacrifice time were based on two-way analysis of variance regression models, including sacrifice time by scaffold size interaction terms to allow investigation of time effects. These models were used to obtain group-specific means and 95% confidence intervals as well as pairwise *t*-test comparisons of means between groups. All analyses were conducted using SAS (version 9.12).

Mechanical testing of transplants

The compressive strength of the scaffolds was determined by performing uniaxial tests on the retrieved scaffolds. To avoid damage, the intact specimens were placed on to the test stage in a direction parallel to the printed planer. Previous studies indicate that the compressive response of the scaffolds is very isotropic.[4] The tests were carried out in air on a universal testing machine at a constant crosshead speed of 1 mm/min. The load–displacement curve was registered during the tests. The compressive strength of the structure was calculated as the maximum applied load divided by the measured square section of the sample.

Identification of donor cells

The human-specific repetitive *alu* sequence, which comprises about 5% of the total human genome, can be applied for identification of human cells.[5] We used *in situ* hybridization for the *alu* sequence to study the origin of tissues formed in the transplants. The digoxigenin-labeled probe specific for the *alu* sequence was prepared by PCR, including 1× PCR buffer (Perkin Elmer), 0.1 mM dATP, 0.1 mM dCTP, 0.1 mM dGTP, 0.065 mM dTTP, 0.035 mM digoxigenin-11-dUTP (Boehringer Mannheim Corp.), 10 pmol of specific primers, and 100 ng of human genomic DNA. The following primers were created on the basis of previously reported sequences[6]: sense, 5′-GTGGCTCACGCCTGTAATCC-3′, and antisense, 5′-TTTTTTGAGACGGAGTCTCGC-3′. The method for *in situ* hybridization of HA containing transplants has been previously described.[3] Sections deparaffinized with xylene and ethanol were immersed in 0.2 N HCl at room temperature for 7 min and then incubated in 1 mg/mL pepsin in 0.01 N HCl at 37°C for 10 min. After washing in phosphate-buffered saline, the sections were treated with 0.25% acetic acid containing 0.1 M triethanolamine (pH 8.0) for 10 min and prehybridized with 50% deionized formamide containing 4× SSC at 37°C for 15 min. The sections were then hybridized with 1 ng/μL digoxigenin-labeled probe in hybridization buffer (1× Denhardt's solution, 5% dextran sulfate, 0.2 mg/mL salmon sperm DNA, 4× SSC, 50% deionized formamide) at 42°C for 3 h after the denaturation step at 95°C for 3 min. After washing with 2× SSC and 0.1× SSC, digoxigenin-labeled DNA was detected by immunohistochemistry using anti-digoxigenin alkaline phosphatase-conjugated Fab fragments (Boehringer Mannheim Corp.). Transplants harvested at 18 weeks were analyzed.

Results

A total of 60 transplants were evaluated, including 20 harvested at 9 weeks, 10 at 18 weeks, 10 at 23 weeks, 10 at 38 weeks, and 10 at 50 weeks.

Histomorphometry demonstrated that a lamellar spacing of 500 μm favored bone formation more than a lamellar spacing of 50, 100, 200, or 1000 μm, for both bone as a fraction of the entire transplant (Fig. 1D) and for bone as a fraction of only the tissue (nonscaffold) component of the transplant (Fig. 1E). Bone formation within the transplant interior was separately assessed at 23 weeks, the study midpoint, by an examination of the central one-ninth of the transplants; again, the 500 μm scaffolds had significantly greater amounts of bone than the other groups (Fig. 1F, G), whereas the 1000 and 200 μm scaffolds had negligible amounts of bone within the center of the transplants.

Transplant histology

Especially among the later transplants, bone formation was extensive, and in many areas, bone associated with individual portions of the scaffold appeared to coalesce, forming extensive regions of lamellar bone in close proximity to the scaffold (Fig. 2A). Older transplants contained abundant hematopoietic tissue and occasional adipocytes, all of which were spatially associated with the new bone (Fig. 2B). A modicum of fibrovascular tissue was found among transplants from 23 weeks onward. Older transplants exhibited near complete filling of the scaffold pores with a combination of bone and hematopoiesis (Fig. 2C). All transplants and peri-transplant tissues were characterized by the absence of an inflammatory reaction. In summary, relative to young (9 week old) transplants, the older (50 week) transplants exhibited reduced amounts of scaffold, increased amounts of bone and hematopoiesis, and loss of fibrous tissue.

Identification of donor cells

The human *alu* gene sequence was used to follow the fate of the transplanted cells. *Alu* served as a marker for donor

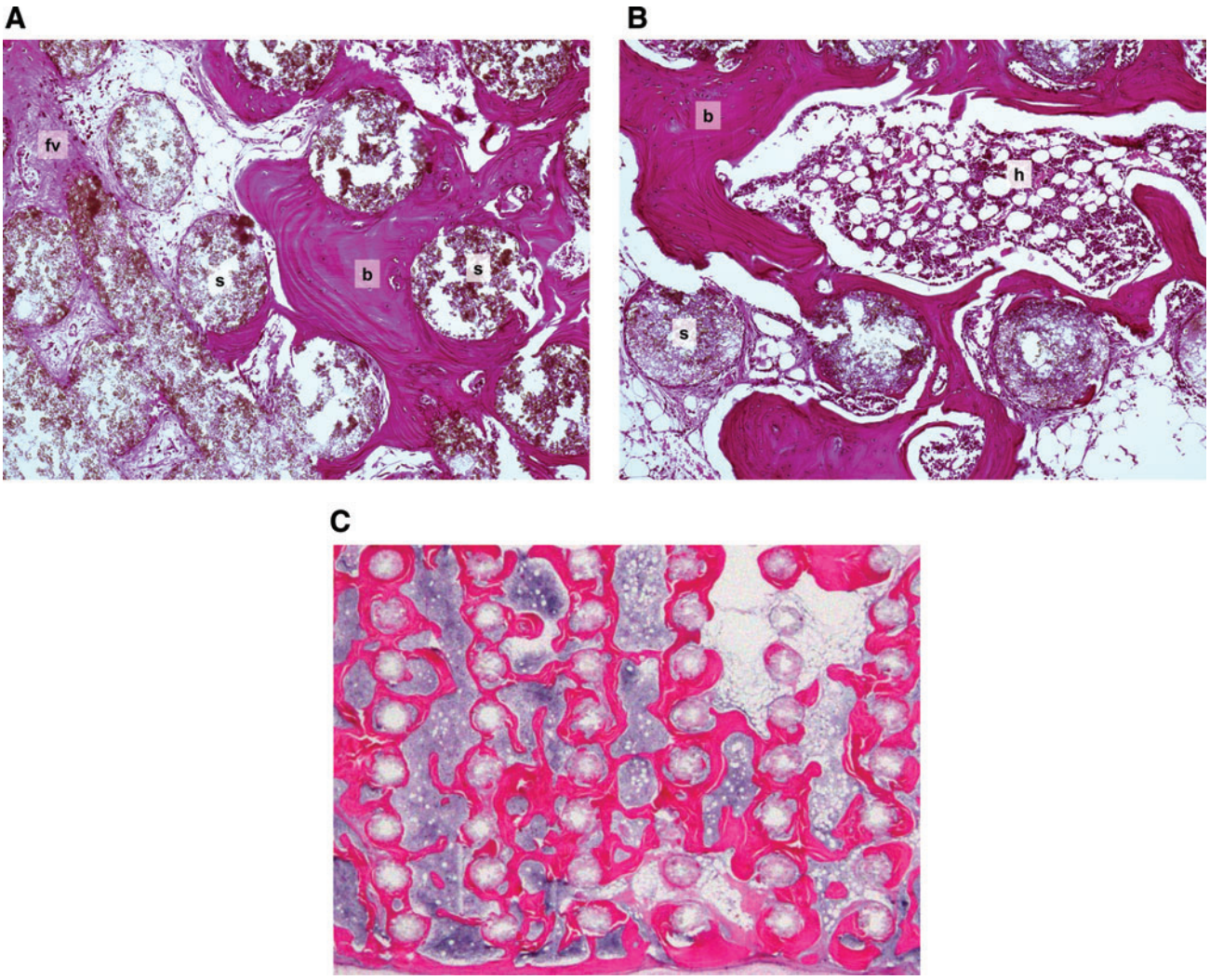

FIG. 2. **(A)** Transplant harvested at 23 weeks, with 100 μm lamellar spacing. Bone is lamellar rather than woven, and is intimately associated with scaffold. Magnification: 20×. **(B)** Transplant harvested at 23 weeks, with 500 μm lamellar spacing. Bone is lamellar. Territories of bone and scaffold encompass regions of hematopoiesis. Magnification: 20×. **(C)** Transplant harvested at 38 weeks, with 500 μm lamellar spacing. Bone fills the majority of nonscaffold spaces in this section. Magnification: 5× (b, bone; fv, fibrovascular tissue; s, scaffold; h, hematopoietic tissue) Stain: hematoxylin and eosin; paraffin embedding following demineralization. Color images available online at www.liebertonline.com/tea

cell activity because it is not present in the mouse recipient cells. Unstained tissue sections from transplants were evaluated with a digoxigenin-labeled probe specific for the *alu* sequence. *Alu* was detected in osteoblasts and osteocytes surrounding the lattice-work of the scaffolds, and was prevalent within and on the newly formed bone in the scaffolds. These findings confirmed that the osteogenic cells were of donor origin rather than originating from the local microenvironment (Fig. 3A–D). Alu was restricted to the new bone and was absent from the peri-transplant tissues. Concurrent positive and negative controls confirmed localization to human cells. These findings were consistent with our earlier studies.[7–9]

Mechanical testing of transplants

In compression testing of fresh scaffolds that were devoid of cells, strength increased 35-fold as pore size decreased from 1000 to 50 μm (Fig. 4A). After 23 weeks in the mice, strength had increased in all scaffolds, consistent with new bone formation. As transplants were harvested at later time points, the relationship between pore size, bone formation, and strength became more complicated. In large pore scaffolds (1000 and 500 μm), strength steadily increased up to the final harvest time point of 50 weeks, in roughly parallel fashion to the amount of newly formed bone. In contrast, strength of small pore scaffolds (100 and 50 μm) steadily decreased after 23 weeks, eventually reaching parity with their pretransplant strength, despite the formation of substantial amounts of bone. This decrease in strength was not associated with any change in the cross-sectional area of the scaffolds (Fig. 4B).

The stress–strain relationships of the fresh scaffold, before cell infiltration, were consistent with a ceramic, showing brittle behavior (Fig. 4C), whereas those relationships among mature transplants, which were extensively infiltrated with fibrovascular tissue and marrow, were more consistent with a plastic.

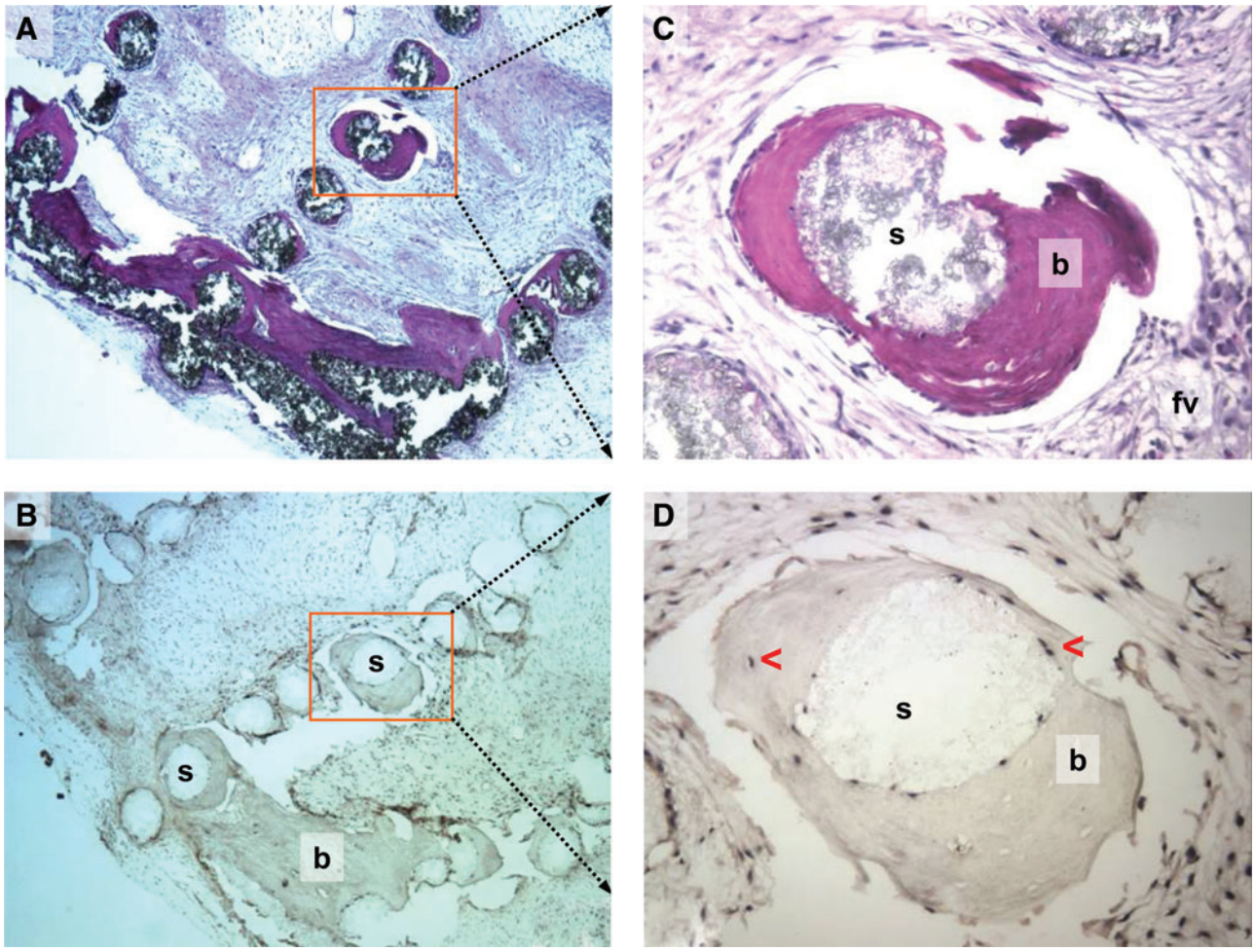

FIG. 3. **(A)** Transplant harvested at 18 weeks, with 1000 μm lamellar spacing. Scaffold lamellae are widely spaced. Bone remains associated with scaffold. Magnification: 5×. **(B)** Histologic section at same location as in **(A)**. Confirmation of the donor origin of the newly formed bone. *In situ* hybridization to *ALU* is localized to osteocytes in the new bone, and is absent in the peri-transplant tissues. Magnification: 5×. **(C)** Higher powered image of histologic section seen in **(A)**. Magnification: 20×. **(D)** Histologic section at same location as in **(C)**. Confirmation of the donor origin of the newly formed bone. *In situ* hybridization to *ALU* is localized to osteocytes in the new bone, and in BMSCs persisting from the time of transplantation. Magnification: 20× (b, bone; s, scaffold; arrows, *alu*-positive cells) Stain **(A, C)**: hematoxylin and eosin; paraffin embedding following demineralization. Color images available online at www.liebertonline.com/tea

Discussion

Particulate and rigid ceramic scaffolds have a role as supports for osteogenic stem cells in bone tissue engineering. Particulate scaffolds, with which our group has greater *in vivo* experience, can be combined *ex vivo* with culture-expanded BMSCs and placed into animal recipients, where they will successfully form bone within 8 weeks.[7,9–13] In nude mice, bone formation can occur with rodent BMSCs or hBMSCs, in either orthotopic or heterotopic locations.[7,13] Such transplants have successfully closed critical-sized calvarial defects in mice and dogs.[1,7] The loose cohesion between particles appears to facilitate nourishment and eventual vascularization of cells within the entire cross section of these transplants, even those as thick as 8 mm.[1] Despite these attractive features, particulate scaffolds' main drawback is their inability to bear mechanical loads during bone formation, making them poor candidates for immediate load-bearing reconstruction of long-bone defects or fractures.

Rigid ceramic scaffolds, in contrast, can be formulated to bear substantial loads from the time of placement. However, earlier rigid scaffolds have not been successful at promoting bone formation by BMSCs because they were unable to balance the competing demands of porosity and strength. Strong scaffolds, for instance, have been too dense to support cell survival; conversely, porous scaffolds maintain cell viability but cannot support loads. Our group is now attempting to develop novel strong scaffolds that simultaneously support cell survival and bone formation.[2,4,14–16]

Despite our initial success, actually understanding how to optimize scaffold geometry, structure, and composition remains a formidable challenge, given the myriad number of parameters that can potentially be optimized. This effort has been somewhat simplified by earlier investigators who focused on improving the osteoconductive properties of rigid

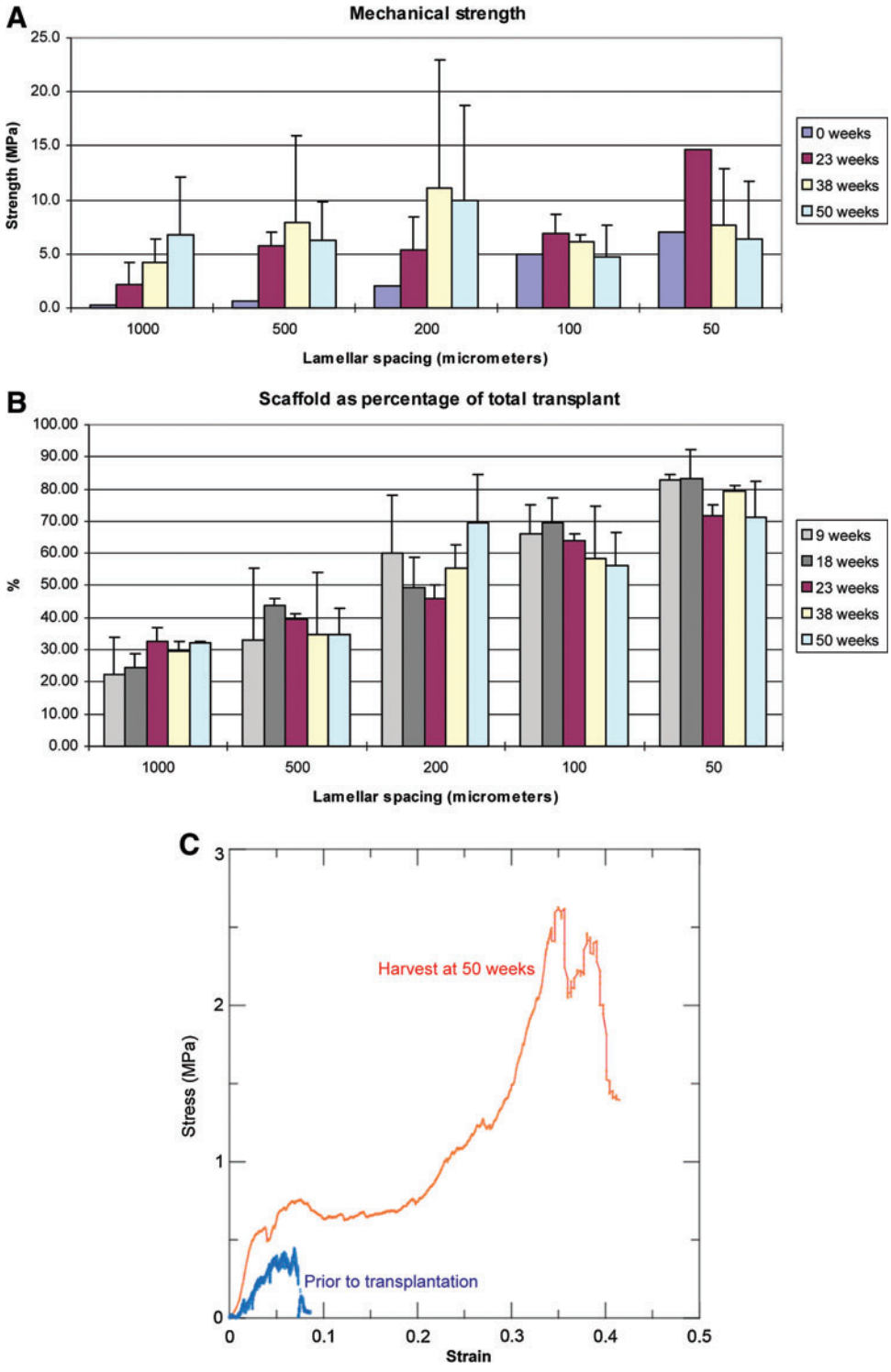

FIG. 4. (A) Compressive strength of the entire transplant, at 0, 23, 38, and 50 weeks. **(B)** Percentage of scaffold within the entire transplant. Transplant periphery and center are both included. **(C)** Stress–strain relationships for 1000 μm scaffold before introduction of cells (blue lower left curve) and following 50 weeks of transplantation (red upper curve). Color images available online at www.liebertonline.com/tea

scaffolds.[17] Those studies typically involved placing the scaffold adjacent to normal bone and then measuring the rate and amount of bone ingrowth into the scaffold. Manipulation of HA and TCP ratios, micro-porosity, macro-porosity, and surface texture have optimized the ability of these scaffolds to support new bone ingrowth. Unfortunately, these studies have typically examined bone formation at the surface of the scaffold rather than at its interior, because they occur over short time-frames, so they could not address questions involving penetration of bone into the scaffold interior. Additionally, none of these studies have included co-transplantation of human osteoprogenitor cells, as our study has.[18–21]

This study was designed to offer several novel sets of observations. First, observations were made over an entire year, rather than the typical 8 to 16 weeks found in most other papers in this field, demonstrating that bone formation continues to increase until at least 38 weeks. Second,

histologic and mechanical observations were made synchronously, demonstrating that they are optimized at different pore sizes, and therefore need to both be measured to better describe the effect of pore size on scaffold performance.

This study was also designed to evaluate the interplay between scaffold surface area and the density of hBMSCs within the scaffold on bone formation. New bone formation first occurs on the scaffold surface, so that scaffolds with substantial surface areas would be expected to promote substantial bone. Yet, linear increases in cell density lead to exponential increases in bone formation, perhaps due to paracrine signaling among the cells, so that scaffolds with substantial voids which were filled with cells would be expected to also promote bone formation. Our study attempted to identify which of these conditions (substantial surface area vs. high cell density) might best promote bone formation. The experiments were thus established with an expectation that cell density in the scaffolds would increase as lamellar spacing increased.

In this study, we created via robo-casting a set of HA scaffolds differing only in the distance between adjacent lamellae. The thickness of the lamellae, their texture, and their microporosity were kept consistent from scaffold to scaffold. We cultured hBMSCs onto the scaffolds *ex vivo* and then transplanted the constructs into nude mice. Scaffolds were observed at time points ranging from 9 to 50 weeks. By histology, bone formation within each scaffold was quantified across the entire cross section and specifically at its interior. *In situ* hybridization was used to confirm a donor source for the bone and osteoblasts. Scaffold strength was measured in the scaffolds before cell seeding and then at 23, 38, and 50 weeks.

We observed bone formation at the first time-point (9 weeks) at the scaffold periphery. With increasing time, overall bone formation increased steadily, proceeding radially inward. Lamellar spacing of 500 μm was most supportive of bone formation at the latest time-points of 38 and 50 weeks in the overall transplant, and especially supported bone formation within the scaffold interior at the intermediate time-point of 23 weeks. The scaffolds also supported the formation of a marrow organ, consistent with our expectations of a bone-supporting scaffold. The osteocytes within the newly formed bone and the osteoblasts lining the bone were confirmed to be of human origin using *in situ* hybridization for *Alu*, and were therefore the transplanted hBMSCs or their progeny. No hBMSCs independent of newly formed were identified, and no cartilage was seen in any section. No tumors were observed in the transplants or elsewhere in the animals, consistent with our 14-year experience transplanting hBMSCs into nude mice.

Transplant compressive strength offered additional insights into scaffold performance. Among fresh scaffolds, compressive strength predictably increased as lamellar spacing decreased. Following transplantation and then harvest at the 23-week time-point, bone had developed in all transplants and was associated with increases in compressive strength in all groups. At later time-points, however, the association between greater bone formation and greater compressive strength was lost, in that transplants with narrow lamellar spacing had diminished strength despite an increase bone formation and no change in scaffold volume. The loss of scaffold strength has two possible explanations—it could be due to a weakening of the inherent scaffold structure over time, most likely due to resorption of the more soluble β-TCP from the scaffold, or it might be due to propagation of micro-fractures within the scaffold.[22] Distinguishing between these two explanations would require additional testing of the transplants in a fresh experiment, perhaps using X-ray microtomography and SEM to quantify the degree of *in vivo* resorption.

In our current study, the compressive strength of our scaffolds reflected an interplay between bone formation and scaffold resorption. It is perhaps not surprising, then, that scaffold histology and mechanical strength do not necessarily coincide—the transplants with the greatest bone formation (500 μm spacing) were not those with the greatest strength (200 μm spacing). These results highlight the importance of using multiple measures of scaffold success (histologic appearance and mechanical performance) to help predict scaffold performance.

An ideal experimental system would permit us to examine the impact of bone formation on scaffold strength separately from the impact of scaffold resorption. Unfortunately, that is difficult to achieve in our model, in which transplanted BMSCs support both bone formation and the formation of a marrow microenvironment; this new marrow in turn may accelerate the scaffold resorption process by introducing osteoclasts to the scaffold. Thus, bone formation supports hematopoiesis, which in turn supports scaffold resorption. The most obvious method for assessing scaffold resorption in the absence of bone formation might have been inclusion of a cell-free transplant in the mouse experiment. While this transplant would have failed to support new bone formation, it would also have failed to form a marrow microenvironment, so it would not undergo as substantial a degree of resorption as a BMSC-imbued transplant.

Our findings support the hypothesis that lamellar spacing helps determine the amount of new bone that forms on HA scaffolds as well as the compressive strength of these scaffolds after 1 year. We speculate that spacing that is too wide may not provide a sufficiently high density of BMSCs to stimulate bone formation,[23] whereas spacing that is too narrow may impede short-term nourishment of the cells and long-term vascular ingrowth. These findings are roughly consistent with those in our prior study using particulate scaffolds, in which particles smaller than 100 μm and larger than 1000 μm promoted markedly less bone formation.[10] The investigation of the specific impact of lamellar spacing on vascular invasion, and the impact of vascular invasion on bone formation, might shed light on these speculations. However, we have observed that successful development of bone cannot occur without adequate vascularization. BMSCs do attract vascularization, so it can be reasonably assumed that in each particular transplant, the degree of bone formation reflects and is supported by the corresponding degree of vascularization. Our findings also suggest that transplant strength represents the result of a complex interplay between new bone formation and scaffold resorption.

Our results suggest that optimization of scaffold geometry, by varying lamellar spacing as we did here, or by varying other parameters such as HA/TCP ratios or surface roughness, may prove sufficient by itself to promote bone formation in the interior of moderately sized rigid scaffolds.

They also begin to offer us insights into the optimal design of large-volume, clinically sized scaffolds.

Acknowledgments

This research was supported in part by the University of California–San Francisco Academic Senate (M.H.M., S.A.), in part by the Bioengineering Research Partnership, NIH/NIDCR 5R01 DE015633 (A.T., E.S., G.W.M., S.M., J.F.), and in part by CTSA UL1 RR024131 (M.H.M.).

Disclosure Statement

No competing financial interests exist.

References

1. Mankani, M.H., Kuznetsov, S.A., Shannon, B., Nalla, R.K., Ritchie, R.O., Qin, Y., and Robey, P.G. Canine cranial reconstruction using autologous bone marrow stromal cells. Am J Pathol **168,** 542, 2006.
2. Franco, J., Hunger, P., Launey, M.E., Tomsia, A.P., and Saiz, E. Direct write assembly of calcium phosphate scaffolds using a water-based hydrogel. Acta Biomater **6,** 218, 2009.
3. Kuznetsov, S.A., Krebsbach, P.H., Satomura, K., Kerr, J., Riminucci, M., Benayahu, D., and Robey, P.G. Single-colony derived strains of human marrow stromal fibroblasts form bone after transplantation *in vivo*. J Bone Miner Res **12,** 1335, 1997.
4. Miranda, P., Pajares, A., Saiz, E., Tomsia, A.P., and Guiberteau, F. Mechanical properties of calcium phosphate scaffolds fabricated by robocasting. J Biomed Mater Res A **85,** 218, 2008.
5. Jacobsen, P.F., and Daly, J. A method for distinguishing human and mouse cells in solid tumors using *in situ* hybridization. Exp Mol Pathol **61,** 212, 1994.
6. Matera, A.G., Hellmann, U., Hintz, M.F., and Schmid, C.W. Recently transposed Alu repeats result from multiple source genes. Nucleic Acids Res **18,** 6019, 1990.
7. Mankani, M.H., Kuznetsov, S.A., Wolfe, R.M., Marshall, G.W., and Robey, P.G. *In vivo* bone formation by human bone marrow stromal cells: reconstruction of the mouse calvarium and mandible. Stem Cells **24,** 2140, 2006.
8. Gronthos, S., Mankani, M., Brahim, J., Robey, P.G., and Shi, S. Postnatal human dental pulp stem cells (DPSCs) *in vitro* and *in vivo*. Proc Natl Acad Sci USA **97,** 13625, 2000.
9. Krebsbach, P.H., Kuznetsov, S.A., Satomura, K., Emmons, R.V., Rowe, D.W., and Robey, P.G. Bone formation *in vivo*: comparison of osteogenesis by transplanted mouse and human marrow stromal fibroblasts. Transplantation **63,** 1059, 1997.
10. Mankani, M.H., Kuznetsov, S.A., Fowler, B., Kingman, A., and Robey, P.G. *In vivo* bone formation by human bone marrow stromal cells: effect of carrier particle size and shape. Biotechnol Bioeng **72,** 96, 2001.
11. Mankani, M.H., Kuznetsov, S.A., Avila, N.A., Kingman, A., and Robey, P.G. Bone formation in transplants of human bone marrow stromal cells and hydroxyapatite-tricalcium phosphate: prediction with quantitative CT in mice. Radiology **230,** 369, 2004.
12. Mankani, M.H., Kuznetsov, S.A., and Robey, P.G. Formation of hematopoietic territories and bone by transplanted human bone marrow stromal cells requires a critical cell density. Exp Hematol **35,** 995, 2007.
13. Mankani, M.H., Kuznetsov, S.A., Marshall, G.W., and Robey, P.G. Creation of new bone by the percutaneous injection of human bone marrow stromal cell and HA/TCP suspensions. Tissue Eng Part A **14,** 1949, 2008.
14. Deville, S., Saiz, E., and Tomsia, A.P. Freeze casting of hydroxyapatite scaffolds for bone tissue engineering. Biomaterials **27,** 5480, 2006.
15. Deville, S., Saiz, E., Nalla, R.K., and Tomsia, A.P. Freezing as a path to build complex composites. Science **311,** 515, 2006.
16. Miranda, P., Pajares, A., Saiz, E., Tomsia, A.P., and Guiberteau, F. Fracture modes under uniaxial compression in hydroxyapatite scaffolds fabricated by robocasting. J Biomed Mater Res A **83,** 646, 2007.
17. Yoshikawa, T., Ohgushi, H., and Tamai, S. Immediate bone forming capability of prefabricated osteogenic hydroxyapatite. J Biomed Mater Res **32,** 481, 1996.
18. Simon, J.L., Michna, S., Lewis, J.A., Rekow, E.D., Thompson, V.P., Smay, J.E., Yampolsky, A., Parsons, J.R., and Ricci, J.L. *In vivo* bone response to 3D periodic hydroxyapatite scaffolds assembled by direct ink writing. J Biomed Mater Res A **83,** 747, 2007.
19. Lan Levengood, S.K., Polak, S.J., Wheeler, M.B., Maki, A.J., Clark, S.G., Jamison, R.D., and Wagoner Johnson, A.J. Multiscale osteointegration as a new paradigm for the design of calcium phosphate scaffolds for bone regeneration. Biomaterials **31,** 3552, 2010.
20. Lan Levengood, S.K., Polak, S.J., Poellmann, M.J., Hoelzle, D.J., Maki, A.J., Clark, S.G., Wheeler, M.B., and Wagoner Johnson, A.J. The effect of BMP-2 on micro- and macroscale osteointegration of biphasic calcium phosphate scaffolds with multiscale porosity. Acta **6,** 3283, 2010.
21. Woodard, J.R., Hilldore, A.J., Lan, S.K., Park, C.J., Morgan, A.W., Eurell, J.A., Clark, S.G., Wheeler, M.B., Jamison, R.D., and Wagoner Johnson, A.J. The mechanical properties and osteoconductivity of hydroxyapatite bone scaffolds with multi-scale porosity. Biomaterials **28,** 45, 2007.
22. Benaqqa, C., Chevalier, J., Saadaoui, M., and Fantozzi, G. Slow crack growth behaviour of hydroxyapatite ceramics. Biomaterials **26,** 6106, 2005.
23. Mankani, M.H., and Yamaguchi, K. American Society for Surgery of the Hand. Seattle, WA: The American Society for Surgery of the Hand, 2007.

Address correspondence to:
Mahesh H. Mankani, M.D.
Department of Surgery
University of California–San Francisco
1001 Potrero Ave., Box 0807
San Francisco, CA 94143-0807

E-mail: mahesh.mankani@ucsf.edu

Received: September 27, 2010
Accepted: February 3, 2011
Online Publication Date: March 31, 2011